Engineering Failure Analysis 142 (2022) 106750

Contents lists available at ScienceDirect

Engineering Failure Analysis

journal homepage: www.elsevier.com/locate/engfailanal

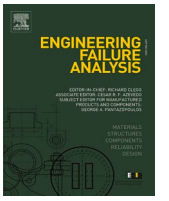

Understanding the behavior of L-type flange joint in wind turbine towers: Proposed mechanisms

Thanh-Tuan Tran [a,b], Daeyong Lee [a,*]

[a] Institute of Offshore Wind Energy, Kunsan National University, 558 Daehak-ro, Jeollabuk-do, Republic of Korea
[b] Renewable Energy Research Institute, Kunsan National University, 558 Daehak-ro, Jeollabuk-do, Republic of Korea

ARTICLE INFO

Keywords:
Wind tower
L-type flange joint
Failure mode
Finite element modeling

ABSTRACT

Generally, collapses of wind turbine towers are caused by bolt ruptures or flange separations at ring flange joints; it is therefore imperative to identify the failure characteristics of bolted ring flange joints. In practical design, traditional approaches primarily focus on bolt failure without paying attention to bolt bending. To handle this limitation, this study aims to examine all possible failure mechanisms of the L-type flange joint used in wind turbine towers. Two independent yielding cases (i.e. yielding in the bolt and yielding in the flange-to-shell junction) and the corresponding plastic tensile resistance are proposed. Numerical simulations of three available L-type flange joints are implemented to verify the accuracy and efficiency of the proposed mechanisms. This study provides a value design framework to predict the load-carrying capacity of flange joints. Combined with existing failure modes, a decision tree that presents possible failure states for bolted flange joints is developed.

Introduction

Ring flange joint with preloaded high strength bolts is the most common solution used to attach wind tower segments to each other [1–6]. During the operating conditions, the flange may be separated or the bolt may be ruptured, leading to the complete failure of the wind tower structure (see Fig. 1). Therefore, it is necessary to understand the performance of the flange joints in practical design.

In the past few decades, researchers have been taking interest in efforts to predict the load-carrying capacity of the flange joint under the tensile force [2,7–9]. Using the analytical and numerical approaches, Madsen *et al.* [8] investigated the ultimate resistance of a bolted flange joint for monopile foundations. Recent projects (i.e, HISTWIN – High-strength tower in steel for wind turbines and HISTWIN2 - High steel tubular towers for wind turbines) suggest a novel methods of joint for wind towers using friction joint with long open slotted holes [10,11]. This newly developed joint considered a competitive alternative for the common flange joints [12,13].

With regard to the development of analytical models for flange joints, several completed works have been reported [14–16]. In light of the plastic theory, Petersen [15] and Seidel [16] proposed simplified models to calculate the ultimate tensile force of flange joints. According to Petersen [15], the main failures in the bolted flange joint can be classified into three different modes: bolt failure (mode A), bolt failure and plastic hinge in flange-to-shell junction (mode B), and plastic hinge in the flange and flange-to-shell junction (mode C). Later, failure mode C was divided into two refined cases by Seidel [16]. The plastic hinges of the flange may occur at the bolt hole center (mode D) or next to the bolt hole center (mode E). Subsequently, another modification was performed by Tobinaga and

* Corresponding author.
E-mail addresses: tranthanhtuan@kunsan.ac.kr (T.-T. Tran), daeyong.lee@kunsan.ac.kr (D. Lee).

https://doi.org/10.1016/j.engfailanal.2022.106750
Received 4 March 2022; Received in revised form 22 August 2022; Accepted 22 August 2022
Available online 27 August 2022

Nomenclature

α	Aspect ratio of the flange, from Tobinaga and Ishihara [-]
α_b	Coefficient factor of between bolt diameter and flange length [-]
β	Coefficient factor of the flange, from Tominaga and Ishihara [-]
γ_{M2}	Resistance factor of the bolt [-]
$\Delta M_{pl,2}$	Increase of moment due to eccentricity of the bolt force [Nmm]
δ_b	Deflection of the flange [mm]
η	Ratio between M_1 and M_2 [-]
θ_b	Rotation of the flange [rad]
λ	Modification factor [-]
ω	Aspect ratio of flange, from this study [-]
$A_{s,b}$	Cross-section of the bolt [mm^2]
a	Distance from bolt center to flange inner [mm]
b	Distance from bolt center to shell center [mm]
$b_E^{'}$	Distance from yielding point of flange to shell center [mm]
c	Width of flange segment [mm]
c'	Reduce segment width [mm]
D	Bolt diameter [mm]
d_h	Diameter of the bolt hole [mm]
d_w	Diameter of washer [mm]
E_b	Elastic modulus of the bolt [N/mm^2]
F_b	Bolt force [N]
F_s	Tensile force [N]
$F_{pl,b}$	Pure plastic force in the bolt [N]
$F_{pl,b,MN}$	Yielding force of bolt considering the interaction of axial force and bending moment [N]
$F_{t,Rd}$	Ultimate force of the bolt [N]
F_u	Ultimate force of the flange segment [N]
$F_{u,A}$	Ultimate force of failure mode A [N]
$F_{u,B}$	Ultimate force of failure mode B [N]
F_{u,B^*}	Ultimate force of failure mode B* [N]
$F_{u,B^{**}}$	Ultimate force of failure mode B** [N]
$F_{u,D}$	Ultimate force of failure mode D [N]
$F_{u,E}$	Ultimate force of failure mode E [N]
$f_{u,b}$	Ultimate strength of bolt [N/mm^2]
$f_{y,b}$	Yielding strength of bolt [N/mm^2]
$f_{y,f}$	Yielding strength of flange [N/mm^2]
$f_{y,s}$	Yielding strength of shell [N/mm^2]
$I_{s,b}$	Moment of inertia of the bolt [mm]
L_b	Bolt length [mm]
M_1	Moment of the flange at the flange-to-shell junction [Nmm]
M_2	Moment of the flange at the bolt axis [Nmm]
$M_{pl,2}$	Plastic moment resistance of the flange [Nmm]
$M_{pl,2}^{'}$	Plastic moment resistance of the flange considering the reduction due to bolt hole [Nmm]
$M_{pl,3}$	Plastic moment resistance of the shell or flange considering the M/N or M/V interaction [Nmm]
$M_{pl,b}$	Pure plastic moment of the bolt [Nmm]
$M_{pl,b,MN}$	Moment of the bolt considering the interaction of axial force and bending moment [Nmm]
$M_{pl,fl}$	Pure plastic moment resistance of the flange [Nmm]
$M_{pl,V,fl}$	Plastic moment of the flange considering M/V interaction [Nmm]
$M_{pl,Tl}$	Pure plastic moment resistance of the shell [Nmm]
$M_{pl,N,Tl}$	Plastic moment of the shell considering M/N interaction [Nmm]
$N_{pl,Tl}$	Pure axial resistance of the shell [N]
$N_{pl,N,Tl}$	Plastic axial resistance of the shell considering M/N interaction [N]
Q	Prying force [N]
s	Shell thickness [mm]
$V_{pl,fl}$	Pure plastic shear resistance of the flange [N]
$V_{pl,V,fl}$	Plastic shear resistance of the flange considering M/N interaction [N]
t_f	Flange thickness [mm]

Ishihara [14] considering the effects of prying force. In this research, when the ratio $\frac{a}{b}$ exceeds 1.25, the equivalent flange inner length $(a^{`})$ is used instead of flange inner length (a). Another research by Couchaux *et al.* [17] examined how the contact between opposite flanges affects on the elastic/plastic behavior of this L-flange joint. At this point, a refined beam model is applied to evaluate the effects of contact between the two flange members.

Regarding the design codes, the following references can be noted: IEC 61400–6 [18] provides guidelines for designing a ring flange joint using the proposed models in Refs. [14–16]. In DNVGL-ST-0126 [3], formulas to design the flange joint are given; however, only the design tensile and shear resistance of individual bolts are provided. GL 2010, Guideline for the Certification of Wind Turbines [19], indicates that the bolt calculations shall be performed based on the DIN 18800 [20] or DNVGL-ST-0126 [3] codes. Other guidelines, such as EN-1993-1-8 (design of joints) [21] and EN-1993-1-9 (fatigue of joints) [22], may be considered; however, they do not specifically address the L-type flange joints.

While fundamental issues related to the evaluation of the load-carrying capacity of the flange joints have been resolved, there are still issues that remain to be addressed. For instance, the conventional failure models consider failure of the bolt without paying attention to the bending effect in the bolt, which has a great influence on the failure of bolt members.

To handle the above limitations, this paper aims to extend the conventional failure mechanisms of L-type flange joints. Two possible cases of yielding (i.e. yielding in the bolt and yielding in the flange-to-shell junction), which are known as the first yielding stage, are presented. The first case (yielding in the bolt) takes into account the effects of bolt bending which allows the inclusion of the additional bolt stresses in the calculations, whereas the second case (yielding in the flange-to-shell junction) caters to the influence of the moment-shear interaction. Combining with the existing failure modes, this study provides the decision tree, which presents possible failure states of a bolted flange joint. In the end, Finite Element Method (FEM) approach was used to verify the accuracy of the developed models. It is found that the proposed failure mechanisms in this study demonstrate a reasonable agreement comparing to the numerical simulations.

Existing failure modeling for ultimate limit state design of L-type flange joints

Various studies on the assessment of the load-carrying capacity of flange joints have been presented. In this section, brief descriptions of the existing analytical models of L-type flange joint are reported.

Assumptions for the ultimate limit state design

- The L-type flange joint is simplified as an individual L-shape segment (single bolt strip segment) under the tensile force (Fig. 2).
- The design loads at the flange joint are equivalent to the tensile force (F_s) acting on the tower shell (Fig. 2b).
- The flange segment without initial imperfection (i.e., no gap between flanges) is considered.
- For ultimate limit state analysis, the preloading force of the bolt is not considered [18].

Petersen model [15]

Petersen's approach [15] is known as the fundamental model to calculate the tensile resistance of the L-flange joint. Based on his research, failure mechanisms of L-flange joints can be divided into three categories (Fig. 3a):

- Failure mode A: bolt failure only
- Failure mode B: bolt failure along with plastic hinge in flange-to-shell junction
- Failure mode C: plastic hinge in flange and flange-to-shell junction

The tensile resistance forces are determined according to the elasto-plastic approach and their values are summarized in Table 1. where

- $F_{t,Rd}$: ultimate force in the bolt

$$F_{t,Rd} = \frac{0.9 f_{u,b} A_s}{\gamma_{M2}} \tag{1}$$

- $M^{`}_{pl,2}$: plastic moment resistance of the flange considering the reduction due to bolt hole, where the reduced segment width is $c^{`} = c - d_h$

$$M^{`}_{pl,2} = \frac{c^{`} t_f^2}{4} f_{y,f} \tag{2}$$

- $M_{pl,3}$: plastic moment resistance of the shell or flange considering the M/N or M/V interaction, respectively, expressed from the following equations:

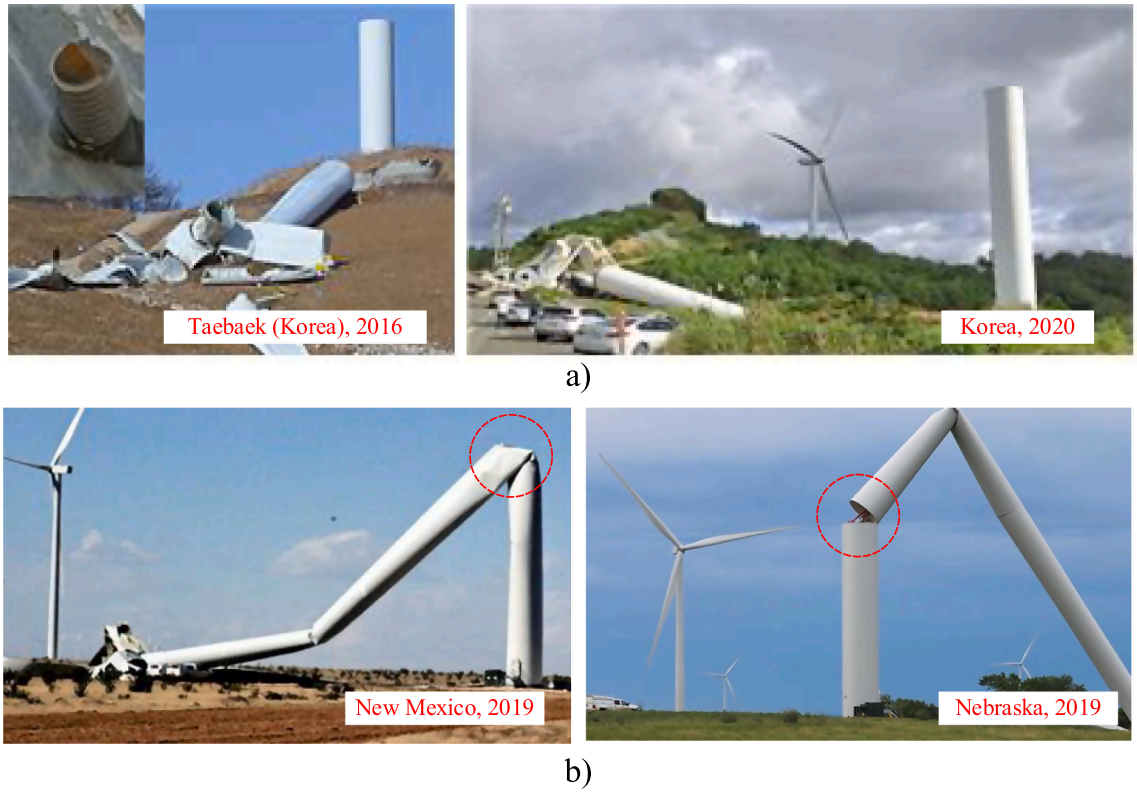

Fig. 1. Failure of Wind Tower: (a) in Korea and (b) Other Parts of the World.

$$M_{pl,3} = min\begin{cases} M_{pl,N,sh} = \left[1 - \left(\frac{N}{N_{pl,sh}}\right)^2\right] M_{pl,sh} = \left[1 - \left(\frac{F_{t,Rd}}{csf_{y,s}}\right)^2\right] \frac{cs^2}{4} f_{y,s} \\ M_{pl,V,fl} = \left[1 - \left(\frac{V}{V_{pl,fl}}\right)^2\right] M_{pl,fl} = \left[1 - \left(\frac{F_{t,Rd}}{ctf\frac{f_{y,f}}{\sqrt{3}}}\right)^2\right] \frac{ct_f^2}{4} f_{y,f} \end{cases} \quad (3)$$

Seidel model [16]

According to Seidel [16], the failure mode C has been divided into two refined cases (Fig. 3b):

- Failure mode D: plastic hinge in the flange at the bolt hole center and flange-to-shell junction
- Failure mode E: plastic hinge in the flange next to the bolt hole center and flange-to-shell junction

The ultimate resistance forces for each failure mode are tabulated in Table 2.
where

- $\Delta M_{pl,2}$: increase in moment due to eccentricity of the bolt force

$$\Delta M_{pl,2} = \frac{F_{t,Rd}}{2} \frac{d_w + d_h}{4} \quad (4)$$

- $M_{pl,2}$: plastic moment resistance of the flange

$$M'_{pl,2} = \frac{ct_f^2}{4} f_{y,f} \quad (5)$$

- $b_E^{'}$: distance from the ultimate force to the yielding point

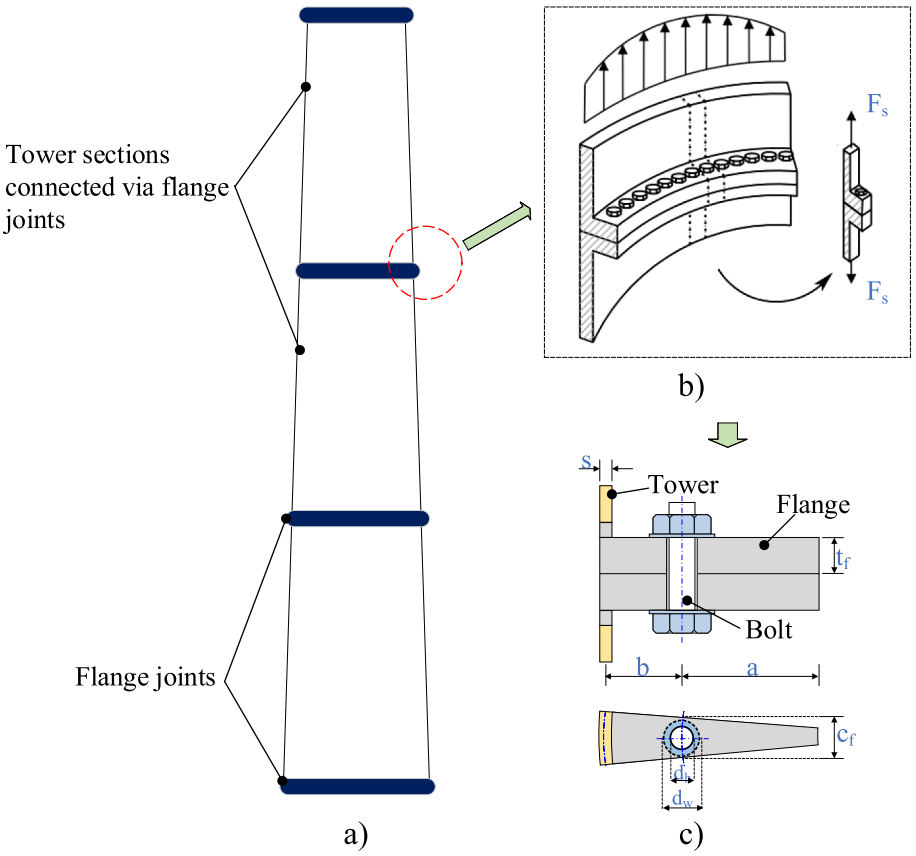

Fig. 2. Diagram of Flange joint: (a) Steel Tower, (b) Segment Approach [16], and (c) Flange Geometry.

$$b_E^{'} = b - \frac{d_w + d_h}{4} \tag{6}$$

Tobinaga and Ishihara model [14]

According to Tobinaga and Ishihara [14], if ratio $\frac{a}{b}$ is higher than 1.25 (see Fig. 2c), the location of the prying force moves to the inner edge of the flange. In this regard, a modification factor λ is recommended so that the effect of prying force may be considered. Therefore, the equivalent flange inner length $(a^{'})$ instead of flange inner length (a) is applied for failure mode B. The ultimate limit capacity is provided in Table 3.

where

$$a^{'} = \lambda a \tag{7}$$

$$\lambda = 1 - \left(1 - \alpha^{\beta}\right)^5 \tag{8}$$

$$\alpha = \frac{t_f}{a+b}; \beta = \left(\frac{a}{b} - 1.25\right)^{0.32} + 0.45 \tag{9}$$

IEC 61400-6 [18]

IEC 61400-6 [18] provides a guideline for the design of a bolted flange joint. The ultimate capacity of the joint may be performed as for a non-preloaded bolted joint. The design process using the existing approaches [14–16] is recommended. The calculation process needs to consider at least three main failure mechanisms described by Petersen [15].

EN 1993-1-8 [21]

According to EN 1993-1-8 [21], the design resistance of bolt member subject to tension is expressed as:

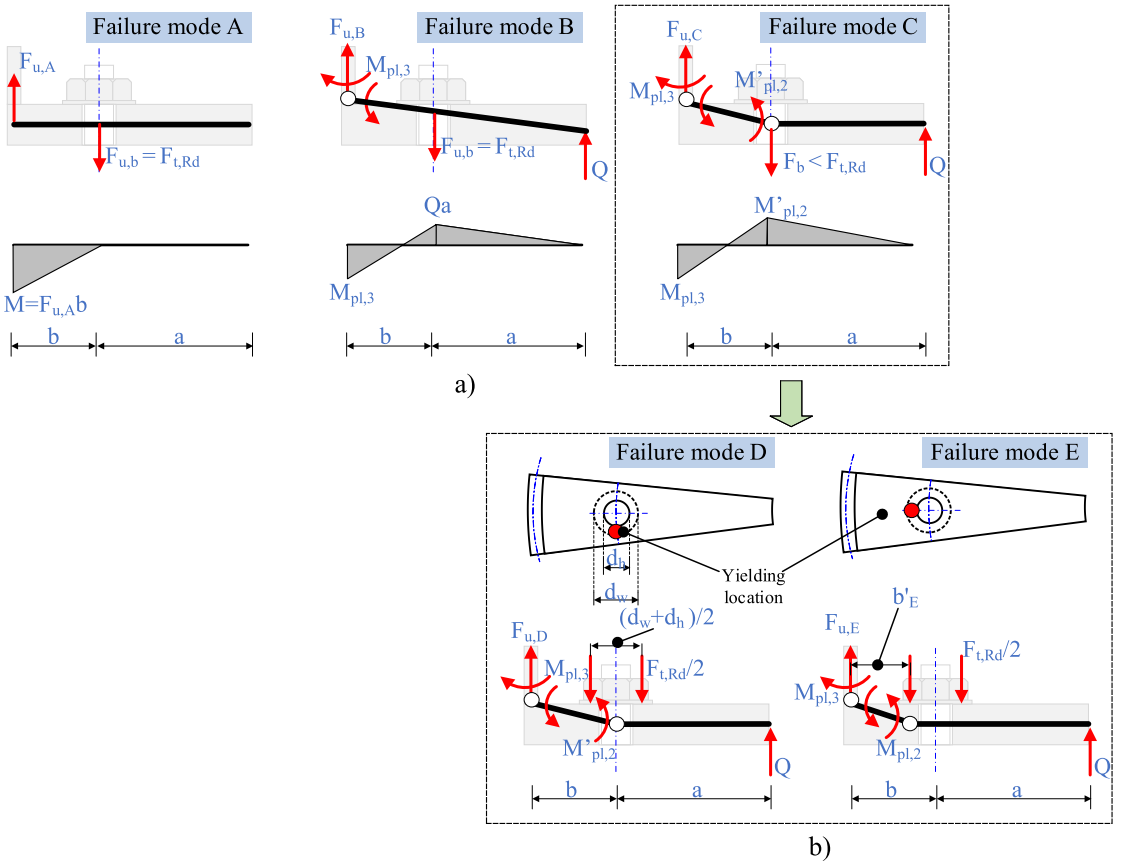

Fig. 3. Failure Mechanisms of L-flange joint: (a) according to Petersen [15] and b) Seidel [16].

Table 1
Ultimate Resistance of L-flange joint According to Petersen [15].

Failure mode	Condition	Ultimate resistance
A	$F_{t,Rd}a \le M_{pl,3}$	$F_{u,A} = F_{t,Rd}$
B	$Qa \le M'_{pl,2}$	$F_{u,B} = \frac{M_{pl,3} + aF_{t,Rd}}{a+b}$
C	$F_s \le F_{t,Rd}$	$F_{u,C} = \frac{M_{pl,3} + M'_{pl,2}}{b}$

Table 2
Ultimate Resistance of L-flange joint According to Seidel [16].

Failure Mode	Condition	Ultimate Resistance
D	$\left(\frac{F_{t,Rd}}{2} - F_{u,D}\right)\left(\frac{d_w + d_h}{4}\right) \le M_{pl,2} - M'_{pl,2}r = \frac{M'_{pl,2} + \Delta M_{pl,2}}{F_{t,Rd} - F_{u,D}} \le a$	$F_{u,D} = \frac{M'_{pl,2} + \Delta M_{pl,2} + M_{pl,3}}{b}$
E	$\left(\frac{F_{t,Rd}}{2} - F_{u,E}\right)\left(\frac{d_w + d_h}{4}\right) \ge M_{pl,2} - M'_{pl,2}r = \frac{M'_{pl,2} + 2\Delta M_{pl,2}}{F_{t,Rd} - F_{u,D}} - \frac{d_w + d_h}{4} \le a$	$F_{u,E} = \frac{M_{pl,2} + M_{pl,3}}{b_E}$

Table 3
Ultimate Resistance of L-flange joint According to Tobinaga and Ishihara [14].

Failure Mode	Conditions	Ultimate Resistance
B	$Qa \le M'_{pl,2}1.25 < \frac{a}{b} \le 2.25\left(-\frac{0.12a}{b} + 0.55\right) \le \alpha \le 1$	$F_{u,B} = \frac{M_{pl,3} + a'F_{t,Rd}}{a' + b}$

$$F_{t,Rd} = \frac{k_2 f_{u,b} A_{s,b}}{\gamma_{M2}} \tag{10}$$

in which $k_2 = 0.9$ and the resistance factor of the bolt $\gamma_{M2} = 1.25$.

New failure modes of L-type flange joints

Shortcomings of the existing approaches

Prying force is important for the flange joint since it has a direct impact on the bolt force [14,17]. In the case of the flange joint, the flange plate is relatively thick; thus, the prying force Q is assumed to be located at the flange edge (Fig. 4). The value of Q can be calculated using the equilibrium conditions. Based on the diagram shown in Fig. 4a, the following equilibrium equations can be used to determine the prying force:

$$Q = F_b - F_u \tag{11}$$

$$M_1 = F_b b - Q(a+b) \tag{12}$$

$$M_2 = Qa \tag{13}$$

where M_1 and M_2 correspond to moments at the flange-to-shell junction and the bolt axis, respectively; F_b and Q correspond to the bolt force and prying force, respectively; and F_u is the ultimate force of the flange segment.

To calculate the bolt force, the parameter η, which can be expressed by the equation $\eta = M_2/M_1$, is introduced. The value of η depends on the failure mode of the flange joints (Fig. 4b). Corresponding to the failure models provided in existing approaches, the value of η is described as follows:

- $0 < \eta < 1$: bolt failure and the plastic hinge at the flange-to-shell junction
- $\eta = 1$: plastic hinge at the bolt or/and the flange-to-shell junction

In Fig. 4b, the first case ($0 < \eta < 1$) typifies the failure mode B. It is worth mentioning that before this failure, yielding at the bolt axis or/and flange-to-shell junction may occur first (Fig. 4c). These yielding stages, which are known as possible failure mechanisms of the L-type flange joints, are not identified separately in the previous studies. This study concerns the development of analytical models to describe the first yielding modes of flange joints. The proposed mechanisms are named as below:

- Failure mode B*: yielding of bolt only.
- Failure mode B**: yielding of flange-to-shell junction only

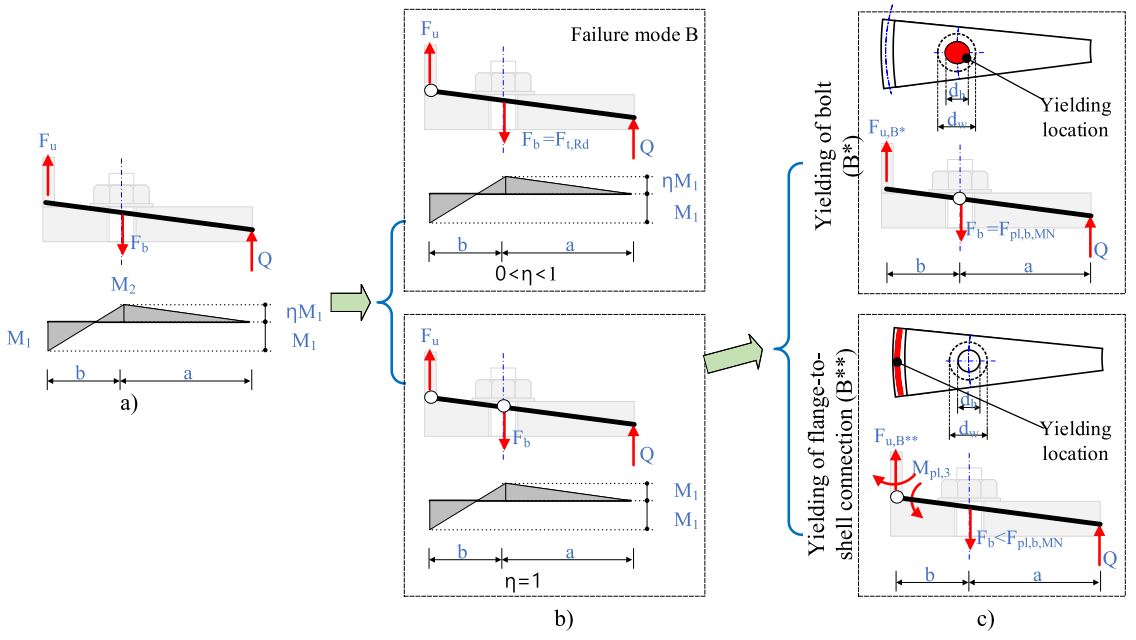

Fig. 4. L-flange joint: (a) Mechanical Model, (b) Value of η, and (c) Proposed Mechanisms.

Formulas for the proposed mechanisms

Yielding of bolt (B)*

Mechanical characteristics of the bolt. Experimental investigations reveal that additional bending in the bolt has great effects on bolt failure [23,24]. However, the existing approaches consider bolt failure without paying attention to this effect. In this study, a simplified evaluation of the influence of bolt bending is presented through defining the plastic section modulus. The plastic moment of the bolt can be calculated with the following formula:

$$M_{pl,b} = \frac{D^3}{6} f_{y,b} \tag{14}$$

where D is the bolt diameter and $\frac{D^3}{6}$ is the plastic modulus of the bolt member.

In terms of the Von Mises yield criterion, the yielding condition for a bolt subjected to axial force and bending moment is given by the following approximation [17]:

$$\frac{M_{pl,b,MN}}{M_{pl,b}} + \left(\frac{F_{pl,b,MN}}{F_{pl,b}}\right)^2 = 1 \tag{15}$$

Where,

$F_{pl,b}$is the pure plastic force in the bolt and is given as:

$$F_{pl,b} = A_{s,b} f_{y,b} \tag{16}$$

where, $A_{s,b}$ is the cross-section of the bolt.

$F_{pl,b,MN}$ and $M_{pl,b,MN}$ are the yielding force and moment in the bolt when considering their interaction. Assuming that the bolt works as a cantilever beam with force and bending moment applied to the top (Fig. 5b), the $F_{pl,b,MN}$ and $M_{pl,b,MN}$ are equal to:

$$F_{pl,b,MN} = \frac{2E_b A_{s,b}}{L_b} \delta_b \tag{17}$$

$$M_{pl,b,MN} = \frac{2E_b I_{s,b}}{L_b} \theta_b \tag{18}$$

where $I_{s,b}$ is the moment of inertia of the bolt.$\left(I_{s,b} = \frac{A_{s,b}^2}{4\pi}\right)$

Under tensile force, the rotation of the flange can be calculated as a rigid beam. Thus, the relationship between rotation (θ_b) and deflection (δ_b) of the flange can be expressed as shown in Fig. 5a:

$$\theta_b \approx tg(\theta_b) = \frac{\delta_b}{a} \tag{19}$$

Using the relation $\alpha_b = \frac{3\pi R_b}{16a} \approx 0.27\frac{d}{a}$ and combining Equations (15)-(18), the bolt force considering the bending effect is given as follows:

$$F_{pl,b,MN} = F_{pl,b}\frac{\sqrt{4+\alpha_b^2} - \alpha_b}{2} \le F_{pl,b} \tag{20}$$

Plastic resistance. This mechanism involves yielding of the bolt; therefore, the bolt force at the plastic condition is taken from Equation (20) $(F_b = F_{pl,b,MN})$. By using the condition $\eta = 1$ and equating Equations (12) and (13), the prying force is computed as:

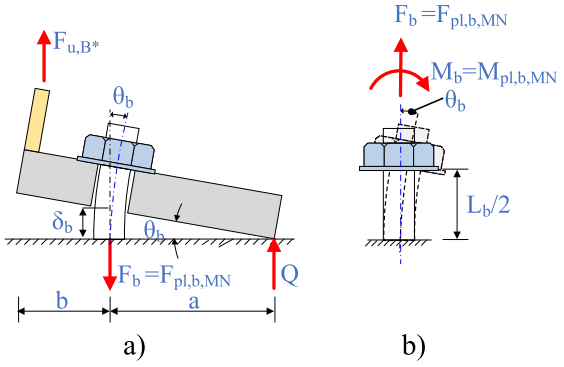

Fig. 5. Deformation of L-flange joint.

$$Q = F_{pl,b,MN}\frac{b}{2a+b} \tag{21}$$

Using the relation $\omega = \frac{a}{b}$, Equation (21) is rewritten as:

$$Q = F_{pl,b,MN}\frac{1}{2\omega+1} \tag{22}$$

Combining Equations (11) and (22), the tensile force that leads to the yielding of the bolts is derived as:

$$F_{u,B^*} = F_{pl,b,MN}\frac{2\omega}{2\omega+1} \tag{23}$$

*Yielding of flange-to-shell junction (failure mode B**)*

Regarding the yielding of the flange-to-shell junction, by equating Equations (12) and (13), the bolt force is computed as:

$$F_b = \frac{2a+b}{ab}M_{pl,3} \tag{24}$$

Combining Equations (11), (13), and (24), the ultimate force that leads to the yielding is expressed as:

$$F_{u,B^{**}} = \frac{2M_{pl,3}}{b} \tag{25}$$

Equation (25) does not consider the influence of the moment-shear interaction on the resistance of bolted flange joint. According to references [17,25], this effect can be taken into account using the Von Mises yield criteria, and it is reproduced as below:

Failure at the flange part. The yielding condition at the flange is given as follows (Appendix A):

$$\frac{M_{pl,V,fl}}{M_{pl,fl}} + \left(\frac{V_{pl,V,fl}}{V_{pl,fl}}\right)^2 = 1 \tag{26}$$

where:

$V_{pl,fl}$ is the pure plastic shear resistance of the flange.

$$V_{pl,fl} = ct_f\frac{f_{y,f}}{\sqrt{3}} \tag{27}$$

$M_{pl,fl}$ is the pure plastic moment resistance of the flange.

$$M_{pl,fl} = \frac{ct_f^2}{4}f_{y,f} = \frac{\sqrt{3}}{4}t_f V_{pl,fl} \tag{28}$$

$M_{pl,V,fl}$ is the plastic moment considering M/V interaction, and it can be expressed from Equation (25):

$$M_{pl,V,fl} = \frac{b}{2}V_{pl,V,fl} \tag{29}$$

By introducing Equations (28)(29) in Equation (26), we have

$$1 - \frac{2b}{\sqrt{3}t_f}\frac{V_{pl,V,fl}}{V_{pl,fl}} - \left(\frac{V_{pl,V,fl}}{V_{pl,fl}}\right)^2 = 0 \tag{30}$$

By re-arranging Equation (30), the ultimate force in the shell is given by:

$$F^1_{u,B^{**}} = V_{pl,V,fl} = V_{pl,fl}\frac{1}{\sqrt{3}}\left[\sqrt{\left(\frac{b}{t_f}\right)^2 + 3} - \frac{b}{t_f}\right] \tag{31}$$

Failure at the shell part. Similarly, the yielding condition at the shell part is given by the following approximation (Appendix B):

$$\frac{M_{pl,N,Tl}}{M_{pl,Tl}} + \left(\frac{N_{pl,N,Tl}}{N_{pl,Tl}}\right)^2 = 1 \tag{32}$$

In which:

- $N_{pl,Tl}$ is the pure plastic axial resistance of the shell

$$N_{pl,Tl} = csf_{y,s} \tag{33}$$

- $M_{pl,Tl}$ is the pure plastic moment resistance of the shell

$$M_{pl,Tl} = \frac{cs^2}{4} f_{y,s} = \frac{s}{4} N_{pl,Tl} \tag{34}$$

- $M_{pl,N,Tl}$ is the plastic moment considering M/N interaction, and it can be expressed from Equations (25):

$$M_{pl,N,Tl} = \frac{b}{2} N_{pl,N,Tl} \tag{35}$$

By introducing Equations (34)(35) in Equation (32), we have

$$1 - \frac{2b}{s}\frac{N_{pl,N,Tl}}{N_{pl,Tl}} - \left(\frac{N_{pl,N,Tl}}{N_{pl,Tl}}\right)^2 = 0 \tag{36}$$

By re-arranging Equation (36), the ultimate force in the shell is given by:

$$F^2_{u,B^{**}} = N_{pl,N,Tl} = N_{pl,Tl}\left[\sqrt{\left(\frac{b}{s}\right)^2 + 1} - \frac{b}{s}\right] \tag{37}$$

Based on Equations (31) and (37), the ultimate resistance at the flange part considering M/V interaction, or ultimate resistance of the shell part considering M/N interaction is given as:

$$F_{u,B^{**}} = min\begin{cases} F^1_{u,B^{**}} = V_{pl,fl}\dfrac{1}{\sqrt{3}}\left[\sqrt{\left(\dfrac{b}{t_f}\right)^2 + 3} - \dfrac{b}{t_f}\right] \\ F^2_{u,B^{**}} = N_{pl,Tl}\left[\sqrt{\left(\dfrac{b}{s}\right)^2 + 1} - \dfrac{b}{s}\right] \end{cases} \tag{38}$$

Ultimate resistance of L-flange joint

In combination with the existing failure models, the final failure modes and ultimate resistance of L-flange joints are summarized in Table 4. The ultimate capacity of L-flange joint is determined as the smallest of the values for the six failure modes:

$$F_u = \min(F_{u,A}, F_{u,B^*}, F_{u,B^{**}}, F_{u,B}, F_{u,D}, F_{u,E}) \tag{39}$$

Furthermore, the decision tree that presents possible failure modes of flange joint is developed (Fig. 6). Within the tree, two proposed failure modes in this work are indicated as the first yielding states of flange joints, followed by four existing failure modes.

Application case studies

Finite element analysis and its verification

Flange geometry

In order to apply the new mechanisms to assess the ultimate capacity of the flange joint, representations of 3 MW, 4 MW, and 5 MW flange joints are considered (Fig. 7). These configurations are currently used in Korean wind farms. The flange and tower shell are

Table 4
Formulas to Predict the Ultimate Resistance of L-flange joint.

Failure Mode	Ultimate Resistance	Reference
A	$F_{u,A} = F_{t,Rd}$	Petersen [15]
B*	$F_{u,B^*} = F_{pl,b}\dfrac{\sqrt{4+\alpha_b^2} - \alpha_b}{2}\dfrac{2\omega}{2\omega+1}$	This study
B**	$F_{u,B^{**}} = min\begin{cases} V_{pl,fl}\dfrac{1}{\sqrt{3}}\left[\sqrt{\left(\dfrac{b}{t_f}\right)^2+3} - \dfrac{b}{t_f}\right] \\ \dfrac{4M_{pl,Tl}}{s}\left[\sqrt{\left(\dfrac{b}{s}\right)^2+1} - \dfrac{b}{s}\right] \end{cases}$	This study
B	$F_{u,B} = \dfrac{M_{pl,3} + aF_{t,Rd}}{a+b}$	Petersen [15]
D	$F_{u,D} = \dfrac{M^*_{pl,2} + \Delta M_{pl,2} + M_{pl,3}}{b}$	Seidel [16]
E	$F_{u,E} = \dfrac{M_{pl,2} + M_{pl,3}}{b_E^*}$	Seidel [16]

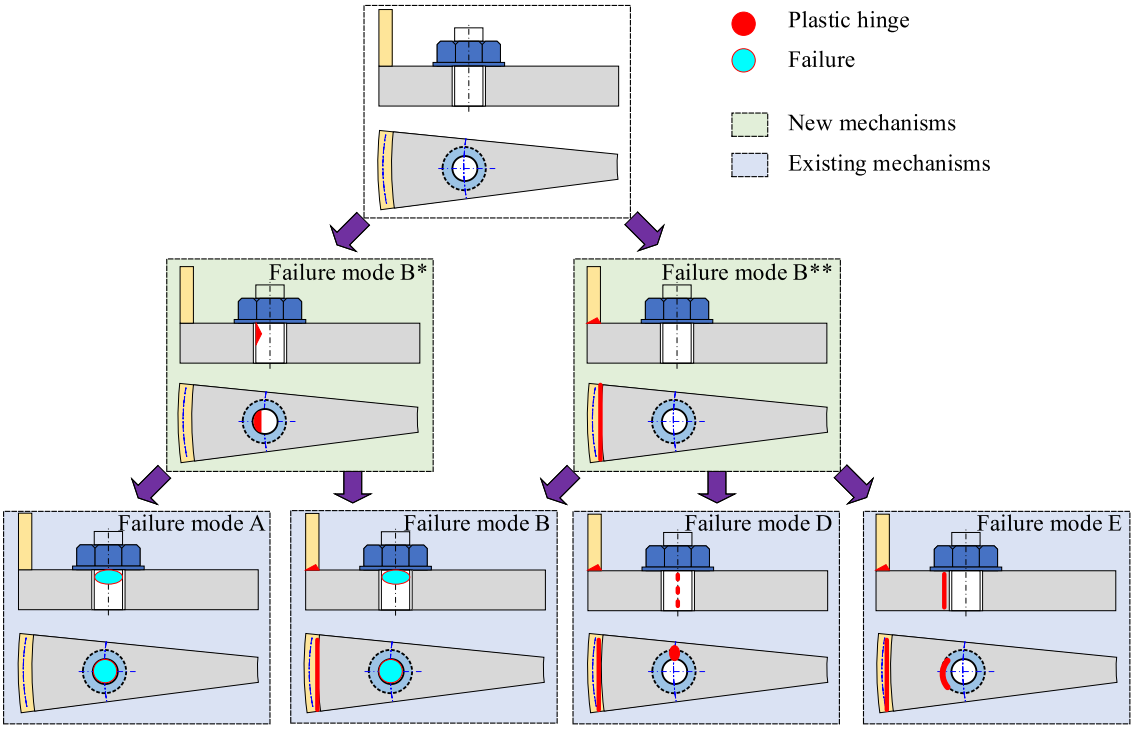

Fig. 6. Decision Tree for Failure Modes of L-flange joint.

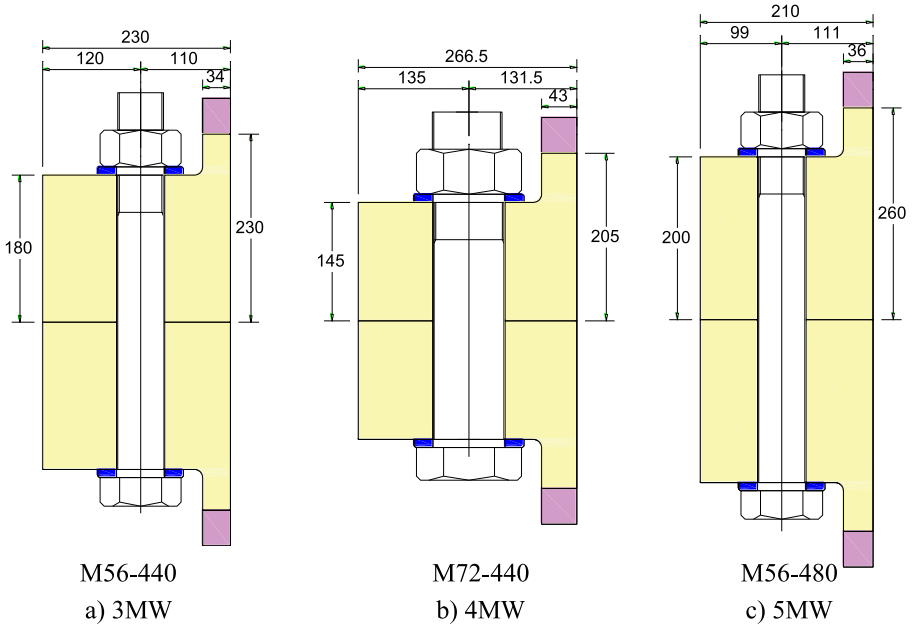

Fig. 7. Flange Geometry Used in This Work.

made of steel with the strength class of S355. The Poisson's ratio and elasticity modulus are 0.3 and 200GPa, respectively. For bolt members, grade 10.9 is used and detailed parameters can be found in the DASt 021 Guideline [26].

Finite element modeling

The prototypes are modeled using the finite element analysis software ANSYS 2022 R1 [27]. A detailed description of the 5 MW flange is shown in Fig. 8. The 3D modeling together with the nonlinear approach is used. All members of the flange joint (i.e., flange,

bolt, and tower shell) are modeled using 3D solid element (Fig. 8a). The bolt with full thread, which can capture the joint stiffness accurately, is modeled. The contact conditions between members, where the nonlinearities may happen, are also defined (Fig. 8b). A frictional coefficient with a value of 0.176 is applied for the contact areas between the two flanges and between bolt and nut [14].

Moreover, the material constitutive with nonlinear behavior is considered to simulate the plastic behavior of the flange joint. In this work, the material models of the flange and tower shell are developed following the DNVGL-RP-C208 Guideline [28], whereas the material constitutive adopted from Kontolati is considered for the 10.9 bolt [29]. The stress–strain curves used in this study are presented in Fig. 9.

Regarding the boundary conditions, the bottom tower is considered to be fixed at all degrees of freedom. Loading conditions for the analysis include two steps: (1) bolt pre-tensioning and (2) tensile loads at the top of the tower shell. The application of bolt pre-tensioning follows the regulation of EN 1993-1-8 [21].

Verification of finite element approach

The FEM approach used in this work is validated using a prototype flange segment with the available test data provided by Seidel and Schaumann [30]. Geometrical parameters of the flange are given in Fig. 10a. The 3D modeling of the test is displayed in Fig. 10b. A comparison of bolt force observed from the FEA and test is reported is given in Fig. 10c. It is seen that the numerical prediction obtained from FEA is close to the experimental test. Thus, the FEM approach can be used for further studies.

Verification of the proposed mechanisms

The accuracy and efficiency of the proposed mechanisms are verified in comparison with those obtained from the existing studies (Section 4.2.1) and numerical simulation (Section 4.2.2).

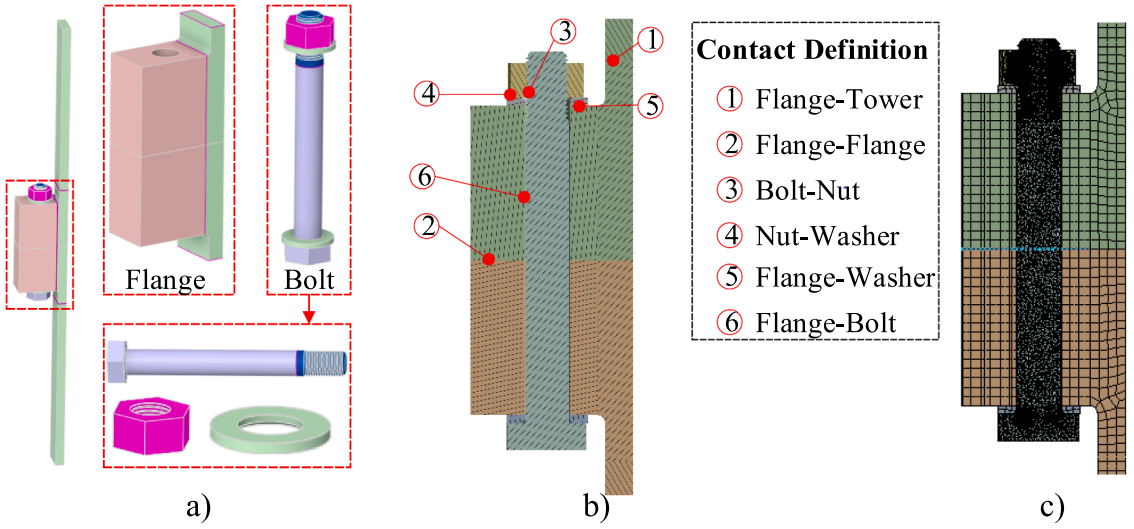

Fig. 8. Finite Element Modeling: (a) Main Components, (b) Contact Conditions, and (c) Global Mesh.

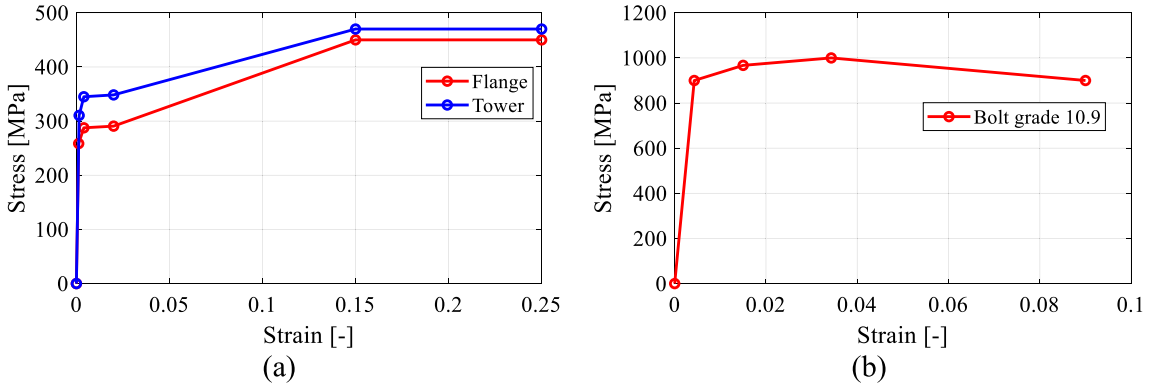

Fig. 9. Constitutive Model of Material: (a) Flange and Tower Shell and (b) Bolt.

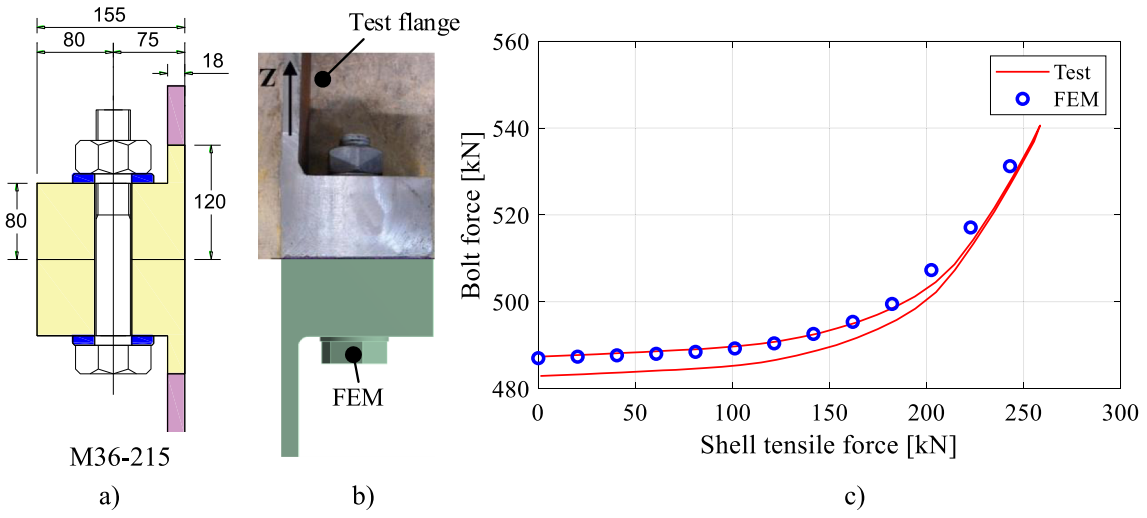

Fig. 10. Seidel Prototype: (a) Geometry, (b) Test Flange and FE model, and (c) Verification.

Ultimate resistance of flange joints

A comparison between the proposed mechanisms and the conventional Petersen/Seidel (P/S) approach is made. Summarization of the resistance forces is presented in Tables 5-6. As seen, the P/S approach (Table 5) shows that mode B is the main failure mode of 3 MW and 5 MW, indicating bolt failure along with plastic hinge in the flange-to-shell junction. Whereas the failure mode D is the governing one in the case of 4 MW. However, considering the proposed mechanisms (see Table 6), yielding in the bolt (mode B*) is the governing failure mode for all flange configurations.

The discrepancy between the proposed and the existing solutions can be explained as follows:

- The ultimate limit state by the P/S approach considers the flange as a beam and the tensile resistances are determined according to the plastic hinge theory. Failure mode B states that the bolt failure and plastic hinge at the flange-to-shell junction may occur; however, it is unclear which location is the governing one.
- In case of the proposed mechanisms, the yielding in the bolt and the yielding in the flange-to-shell junction are separately identified. The bolt yielding considers the influence of the axial force and bending moment, while the flange-to-shell yielding considers the influence of the shear force-bending moment interaction. These are important since they can lead to an increase in the plastic resistance.

Comparison between proposed mechanisms and numerical solutions

According to the basic assumptions given in Section 2.1, the analytical model is developed without considering the preloading force; thus, numerical models without preloaded bolts are also considered [15,16,18]. Different sensitive positions of the flange joint, as shown in Fig. 11, are studied in the analysis. These points (i.e., A, B and C) represent the areas where the yielding may occur.

Table 5
Failure Mode of Flange joints: Existing Failure Mechanisms.

Specimen		**3 MW**	**4 MW**	**5 MW**
Ultimate Resistance (N)	$F_{u,A}$	1.90E + 06	3.24E + 06	1.90E + 06
	$F_{u,B}$	1.04E + 06	1.65E + 06	9.40E + 05
	$F_{u,D}$	2.14E + 06	1.26E + 06	2.17E + 06
	$F_{u,E}$	5.21E + 06	2.71E + 06	5.81E + 06
	F_{ult}	1.04E + 06	1.26E + 06	9.40E + 05
Failure Mode		**B**	**D**	**B**

Table 6
Failure Mode of Flange joints: Considering Proposed Mechanisms.

Specimen		**3 MW**	**4 MW**	**5 MW**
Ultimate Resistance (N)	$F_{u,A}$	1.90E + 06	3.24E + 06	1.90E + 06
	$F_{u,B}$	1.04E + 06	1.65E + 06	9.40E + 05
	F_{u,B^*}	1.79E + 05	2.35E + 05	1.69E + 05
	$F_{u,B^{**}}$	2.26E + 05	3.25E + 05	2.85E + 05
	$F_{u,D}$	2.14E + 06	1.26E + 06	2.17E + 06
	$F_{u,E}$	5.21E + 06	2.71E + 06	5.81E + 06
	F_{ult}	2.26E + 05	3.25E + 05	2.85E + 05
Failure Mode		**B***	**B***	**B***

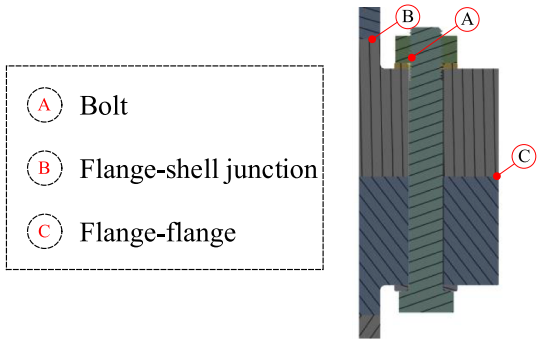

Fig. 11. Selected Positions.

A comparison of axial stress observed from these sensitive points is given in Fig. 12. As seen, the axial stress increases with an increase in the tensile load, and the response is linear until reaching the yielding point. Another finding is that yieldings of all configurations happen in the bolt that is known as the first yielding point. Using these $F_z - \sigma$ diagrams, the resistance force (defined as Fu_{FEM}) is predicted and their values are summarized in Table 7.

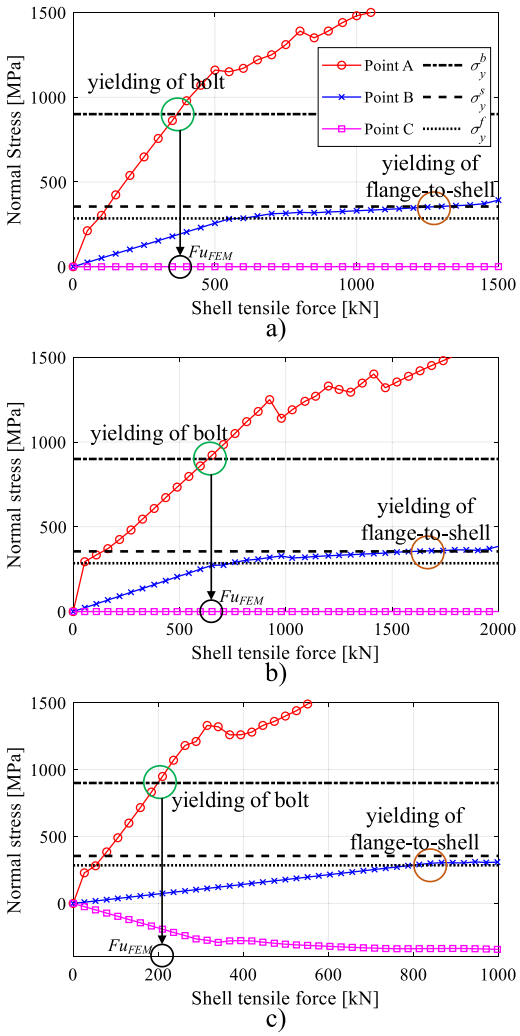

Fig. 12. Axial Stress in Flange joints: (a) 3 MW, (b) 4 MW, and (c) 5 MW.

Table 7
Ultimate Resistance of Flange joints.

	Fu_{FEM} (N)	$Fu_{P/S}$(N)	$Fu_{thisstudy}$(N)
3 MW	3.7E + 05	1.04E + 06	2.26E + 05
4 MW	6.2E + 05	1.26E + 06	3.25E + 05
5 MW	2.0E + 05	9.40E + 05	2.85E + 05

The accuracy of the proposed analytical approach is evaluated against those of existing P/S and numerical solutions, which is plotted in Fig. 13a. In the figure, the dash, dash-dot, and dot vertical lines correspond to the tensile resistance loads obtained from the $Fu_{thisstudy}$, Fu_{FEM} and $Fu_{P/S}$ approaches, respectively, and their resistance values are given in Table 7. It is found that the tensile resistances obtained from the proposed solution are underestimated, whereas those obtained from the P/S approach are overestimated in comparison to the numerical simulations. In addition, the outcomes observed from the proposed solution are closer than the existing P/S approach. The maximum differences between Fu_{FEM} and $Fu_{thisstudy}$ are 51.7 %, 62.1 %, and 15.6 % for 3 MW, 4 MW, and 5 MW, respectively, whereas values between Fu_{FEM} and $Fu_{P/S}$ show the differences of up to 182.0 %, 102.7 %, and 370.2 % for 3 MW, 4 MW, and 5 MW, respectively. The discrepancy between analytical and numerical simulations is due to the following effects:

- The misidentification of the coefficient of friction in the flange/flange and bolt/nut in the analytical model.
- The analytical solution does not cater for the effect of the threaded bolt.

More details of the axial stress distribution in the bolt with different approaches are shown in Fig. 13b. In general, the bending

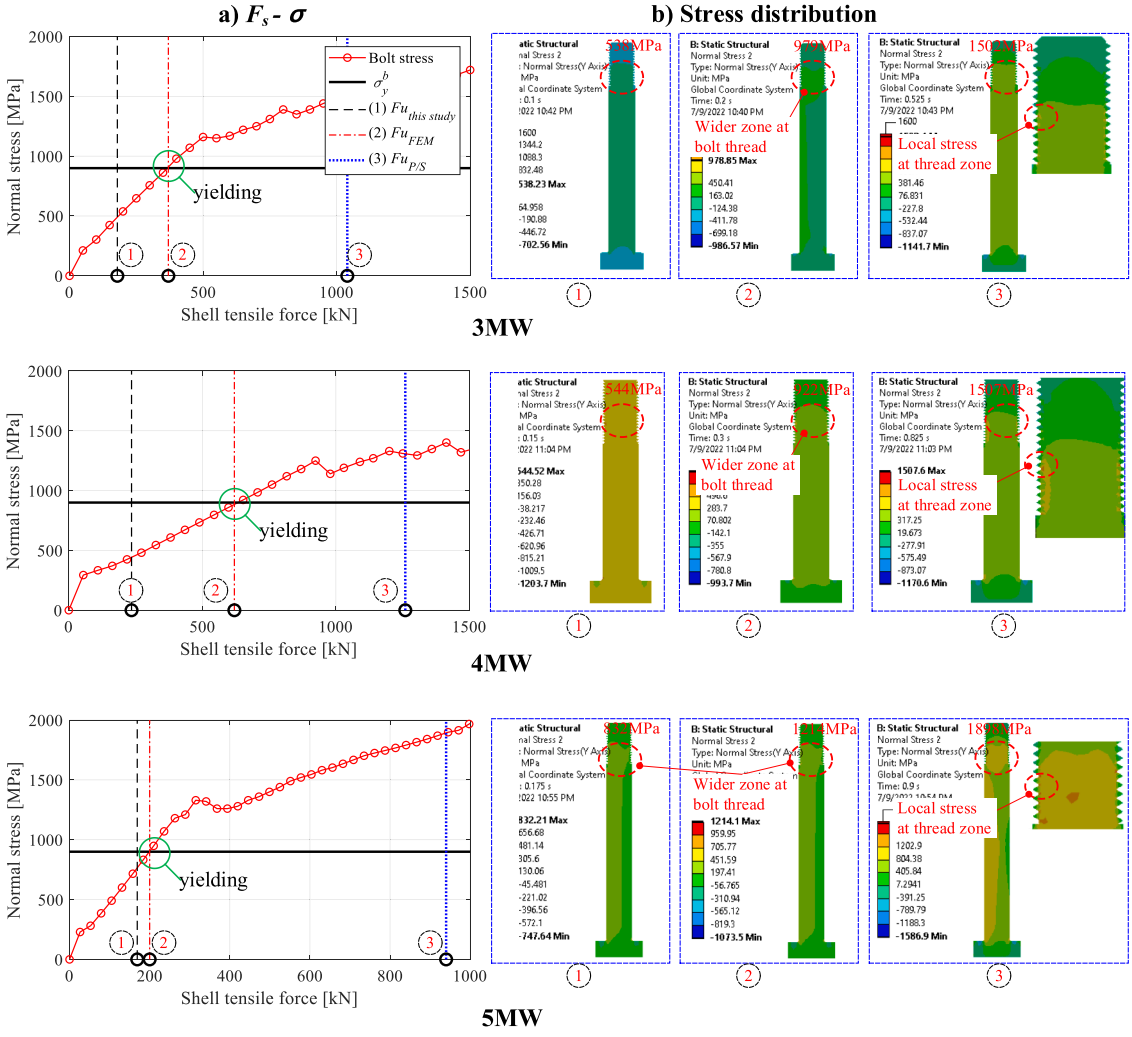

Fig. 13. Axial Stress in Bolt: (a) $F_z - \sigma$ Diagram and (b) Stress Distribution.

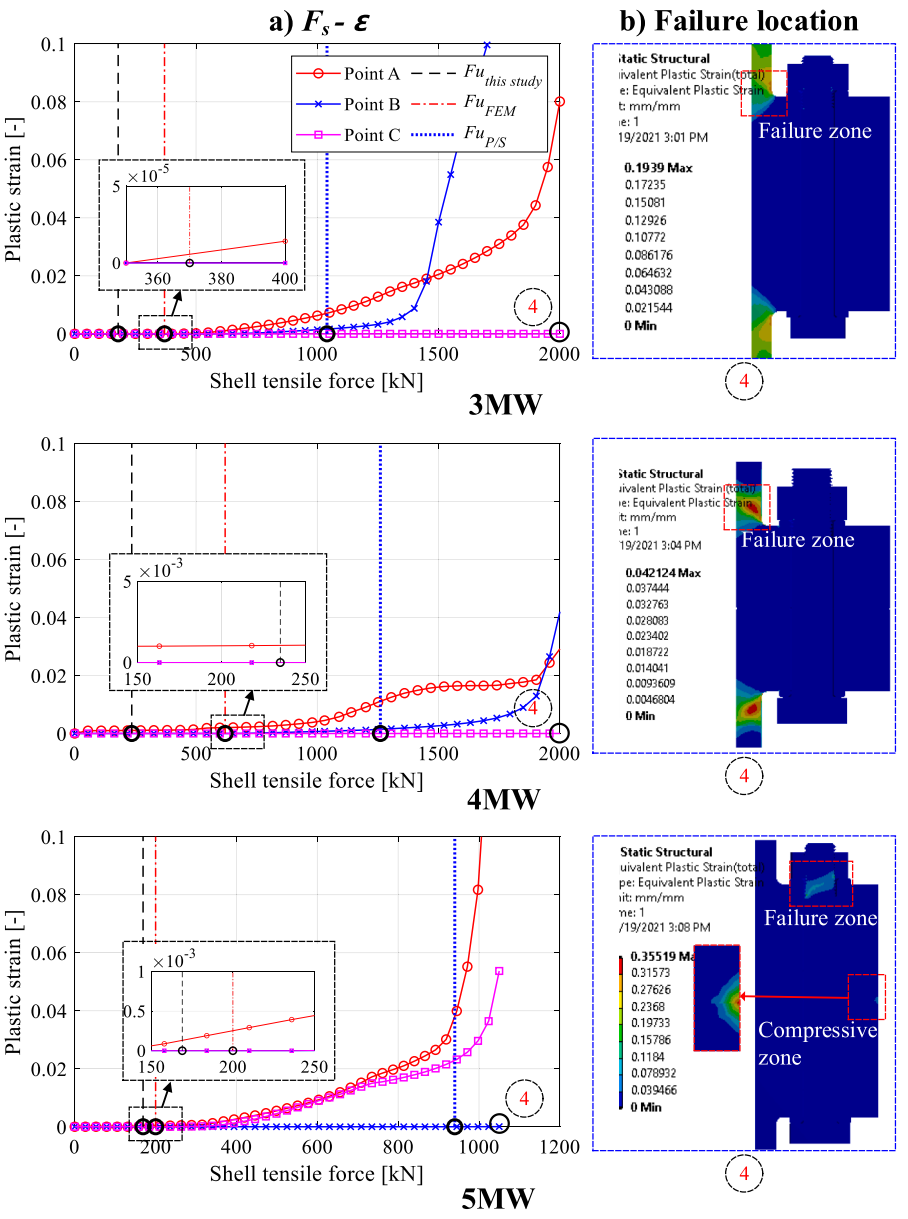

Fig. 14. Plastic Strain: (a) $F_z - \varepsilon$ Diagram and (b) Failure Mode.

moment will induce the stress and produce higher stress at the left side of the bolt, which is visible by creating the cross-section through the axial bolt. Another finding is that the high stress concentrates on the bolt thread for all cases. However, in case of the P/S approach, a wider region of stress distribution is found and they are much higher than the material yield strength limit, with the factors of 1.5 (3 MW and 4 MW) and 1.9 (5 MW).

Further investigation on the strain distribution is also reported to clear the above finding. It is noted that plastic strain in the flange joint occurs when the material is yielding. A comparison of strains in the bolt is presented in Fig. 14. Like the stress, bolt strain is a function of the shell tensile load and increases with the increase in the tensile load. The $F_z - \varepsilon$ diagrams in Fig. 14a indicate how the plastic strain in the sensitive positions develops. An important finding is that the failure mode of flange joints may change due to the incremental tensile force. When loading to 1450kN for 3 MW and 1900kN for 4 MW, the plastic strain in the bolt increases along with the increase of tensile force, whereas there is a slight change at the flange-to-shell junction. As the tensile force is continuously increased (up to 2000kN), the plastic strain at the flange-to-shell junction increases rapidly, leading to the failure of flange joints. Details of the final failure can be seen in Fig. 14b.

With regards to the 5 MW, an important finding is that there is no yielding at the flange-to-shell junction. The plastic strain occurs at

the bolt (position A) and flange tips (position C). It is noted that the yielding at the internal flange tip is a consequence of the compressive stress caused by the separation of flange members. This failure mode is not important compared to other failures in the flange design. In the case of bolt member (position B), the failure occurs at the threaded zone. As seen, a wide zone of plastic deformation goes through the bolt section, leading to the failure of flange joint (Fig. 14b).

Conclusions

This study examines all possible failure mechanisms of the L-type flange used in wind turbine towers. Two yielding cases (i.e. yielding in the bolt and yielding in the flange-to-shell junction) are recommended and the corresponding design formulations to calculate the ultimate resistance of the flange joint are proposed. The effect of bolt bending, which causes additional stresses in the bolt, is discussed. Combining these cases with the previous studies, the decision tree representing all possible failure modes of the flange joint is developed.

The proposed failure mechanisms are developed based on the general assumptions of the existing approach, in which the flange model is considered as a rigid beam. Therefore, the developed modes are consistent with the current approaches. Furthermore, they provide an efficient estimation to predict the yielding point in the flange joints due to their simplicity.

With the use of finite element analyses, the outcomes calculated from the proposed models are verified based on three available flange joints. Results indicate that it is necessary to include bolt bending in the calculation of the ultimate resistance of the flange joint in order to increase design safety of the flange joint.

Declaration of Competing Interest

The authors declare that they have no known competing financial interests or personal relationships that could have appeared to influence the work reported in this paper.

Data availability

The authors do not have permission to share data.

Acknowledgments

This research was supported by Basic Science Research Program through the National Research Foundation of Korea (NRF) funded by the Ministry of Education (NRF2021R1A6A1A0304518511) and by Korea Electric Power Corporation (Grant Number: R21XO01-39).

Appendix A:. Yielding condition at the flange part

According to Fig. A1, the reduced plastic moment resistance of the flange is expressed by:

$$M_{pl,V,fl} = \int_s \sigma dS = x(t_f - x)cf_{y,f} \tag{A.1}$$

The reduced plastic force resistance of the flange is expressed by:

$$V_{pl,V,fl} = \int_s \tau dS = (t_f - 2x)c\tau_{y,f} \tag{A.2}$$

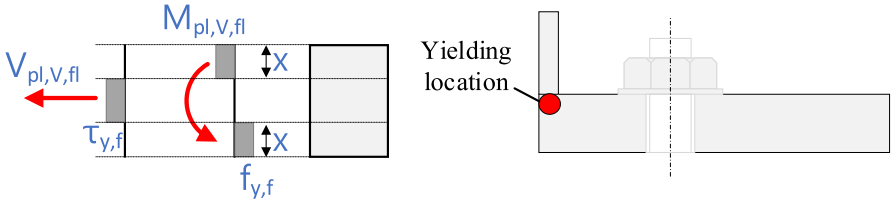

Fig. A1. Distribution of plastic stress in the flange.

$$\tau_{y,f} = f_{y,f}/\sqrt{3}$$

By introducing Eq. (A.2) in Eq. (A.1), the reduced plastic moment resistance of the flange is derived as:

$$M_{pl,V,fl} = M_{pl,fl} - \frac{3V_{pl,V,fl}^2}{4cf_{y,f}} \tag{A.3}$$

Combining Eqs. (27)(28), we have.

$$M_{pl,Fl} = \frac{\sqrt{3}}{4} t_f V_{pl,Fl} \tag{A.4}$$

Combining Eqs. (A.3)(A.4), we have.

$$\frac{M_{pl,V,fl}}{M_{pl,fl}} + \left(\frac{V_{pl,V,fl}}{V_{pl,fl}}\right)^2 = 1 \tag{A.5}$$

Appendix B:. Yielding condition at the shell part

According to Fig. B1, the reduced plastic moment resistance of the shell is expressed by:

$$M_{pl,N,Tl} = \int_s \sigma dS = x(s-x)cf_{y,s} \tag{B.1}$$

The reduced plastic force resistance of the shell is expressed by:

$$N_{pl,N,Tl} = \int_s \sigma dS = (s-2x)cf_{y,s} \tag{B.2}$$

By introducing Eq. (B.2) in Eq. (B.1), the reduced plastic moment resistance of the shell is derived as:

$$M_{pl,N,Tl} = M_{pl,Tl} - \frac{N_{pl,V,fl}^2}{4cf_{y,f}} \tag{B.3}$$

Combining Eqs. (33)(34), we have

$$M_{pl,Tl} = \frac{1}{4} s N_{pl,Tl} \tag{B.4}$$

Combining Eqs. (B.3)(B.4), we have

$$\frac{M_{pl,N,Tl}}{M_{pl,Tl}} + \left(\frac{N_{pl,N,Tl}}{N_{pl,Tl}}\right)^2 = 1 \tag{B.5}$$

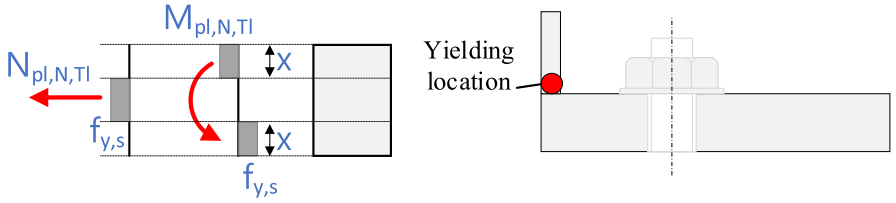

Fig. B1. Distribution of plastic stress in the shell.

References

[1] C. Petersen, Tragfähigkeit Imperfektionsbehafteter Geschraubter Ringflansch-Verbindungen, 1990.
[2] P. Schaumann, M. Seidel, Failure analysis of bolted steel flanges, Struct. Fail. Plast. (2000) 507–512, https://doi.org/10.1016/B978-008043875-7/50211-2.
[3] DNVGL-ST-0126, Support Structures for Wind Turbines, 2018.
[4] T.T. Tran, E. Kim, D. Lee, Development of a 3-legged jacket substructure for installation in the southwest offshore wind farm in South Korea, Ocean Eng. 246 (2022), 110643, https://doi.org/10.1016/J.OCEANENG.2022.110643.
[5] T.-T. Tran, S. Kang, J.-H. Lee, D. Lee, Directional bending performance of 4-leg jacket substructure supporting a 3MW offshore wind turbine, Energies 14 (2021) 2725, doi: 10.3390/EN14092725.
[6] M. Alonso-Martinez, J.M. Adam, F.P. Alvarez-Rabanal, J.J. del Coz Díaz, Wind turbine tower collapse due to flange failure: FEM and DOE analyses, Eng. Fail. Anal. 104 (2019) 932–949, doi: 10.1016/J.ENGFAILANAL.2019.06.045.
[7] C. Heistermann, Resistance of Friction Connections with Open Slotted Holes in Towers for Wind Turbines, Luleå University of Technology, 2014.
[8] C.A. Madsen, J.C. Kragh-Poulsen, K.J. Thage, M.J. Andreassen, Analytical and numerical investigation of bolted steel ring flange connection for offshore wind monopile foundations, IOP Conf. Ser. Mater. Sci. Eng. 276 (2017), 012034, https://doi.org/10.1088/1757-899X/276/1/012034.
[9] J.-S. Chou, W.-T. Tu, Failure Analysis and Risk Management of a Collapsed Large Wind Turbine Tower, Eng. Fail. Anal. 18 (1) (2011) 295–313.
[10] M. Veljkovic, C. Heistermann, W. Husson, M. Limam, M. Feldmann, High-Strength Tower in Steel for Wind Turbines (HISTWIN), 2009.
[11] C.; Heistermann, J. Siltanen, M. Veljkovic, S. Gerasimidis, High Steel Tubular Towers for Wind Turbines (HISTWIN2), 2015.
[12] M. Pavlović, C. Heistermann, M. Veljković, D. Pak, M. Feldmann, C. Rebelo, L.S. Da Silva, Connections in towers for wind converters, Part I: Evaluation of down-scaled experiments, J. Constr. Steel Res. 115 (2015) 445–457, https://doi.org/10.1016/J.JCSR.2015.09.002.
[13] M. Pavlović, C. Heistermann, M. Veljković, D. Pak, M. Feldmann, C. Rebelo, L.S. Da Silva, Connections in towers for wind converters, Part II: The friction connection behaviour, J. Constr. Steel Res. 115 (2015) 458–466, https://doi.org/10.1016/J.JCSR.2015.05.009.
[14] I. Tobinaga, T. Ishihara, A study of action point correction factor for L-type flanges of wind turbine towers, Wind Energy 21 (9) (2018) 801–806, https://doi.org/10.1002/we.2193.
[15] C. Petersen, Stahlbau, Stahlbau. (2013), https://doi.org/10.1007/978-3-8348-8610-1.
[16] M. Seidel, Zur Bemessung Geschraubter Ringflanschverbindungen Von Windenergieanlagen, Leibniz Universität Hannover, Germany, 2001, doi: 10.13140/RG.2.2.14685.36328.
[17] M. Couchaux, M. Hjiaj, I. Ryan, A. Bureau, Tensile resistances of L-stubs, J. Constr. Steel Res. 138 (2017) 131–149, https://doi.org/10.1016/J.JCSR.2017.06.016.
[18] IEC 61400-6, IEC 61400-6: Wind Energy Generation System - Part 6: Tower and Foundation Design Requirements, 2020.
[19] Germanischer Lloyd, GL 2010-Guideline for the Certification of Wind Turbines, 2010. Available from: <www.gl-group.com/GLRenewables>.
[20] Deutsches Institut fur Normung E.V. (DIN), DIN 18800-1: Steel Structures - Part 1: Design and Construction, 2008.
[21] European Standard, EN-1993-1-8: Eurocode 3: Design of Steel Structures - Part 1-8: Design of Joints, 2011.
[22] European Standard, EN-1993-1-9: Eurocode 3: Design of Steel Structures - Part 1-9: Fatigue, 2011.
[23] F. Huang, D. Zhang, W. Hong, B. Li, Mechanism and calculation theory of prying force for flexible flange connection, J. Constr. Steel Res. 132 (2017) 97–107, https://doi.org/10.1016/j.jcsr.2017.01.014.
[24] H.Z. Deng, C. Li, X.Q. Song, F. Li, P.C. Fu, Tensile resistance and design model of an external double-layered flange connection, J. Constr. Steel Res. 161 (2019) 309–327, https://doi.org/10.1016/J.JCSR.2019.07.013.
[25] C. Faella, V. Piluso, G. Rizzano, Structural Steel Semirigid Connections : Theory, Design, and Software, CRC Press, 1999.
[26] Deutscher Ausschuss für Stahlbau, DASt-Richtlinie 021: Schraubenverbindungen Aus Feuerverzinkten Garnituren M39 bis M72., 2013.
[27] ANSYS, ANSYS®Academic Research Mechanical, Release 2022.R1, Help System, Coupled Field Analysis Guide, ANSYS, Inc, 2022.
[28] DNVGL, DNVGL-RP-C208: Determination of Structural Capacity by Non-Linear Finite Element Analysis Methods - DNV, 2013.
[29] K. Kontolati, Numerical Investigation Of Weak-Axis I Profile Connections, Univesity of Thessaly (2017).
[30] M. Seidel, P. Schaumann, Measuring Fatigue Loads of Bolts in Ring Flange Connections, in: Eur. Wind Energy Conf., 2001.